

Probing top quark electromagnetic dipole moments in single-top-plus-photon production

M. Fael^{1,2} and T. Gehrmann¹

¹*Institut für Theoretische Physik, Universität Zürich, Winterthurerstrasse 190, CH-8057 Zürich, Switzerland*

²*Dipartimento di Fisica e Astronomia, Università di Padova and INFN, Sezione di Padova, via Marzolo 8, I-35151 Padova, Italy*

(Received 12 July 2013; published 8 August 2013)

The production of a single top quark in association with an isolated photon probes the electromagnetic coupling structure of the top quark. We investigate the sensitivity of kinematical distributions at the LHC in single-top-plus-photon production in view of a detection of anomalous electric and magnetic dipole moments of the top quark.

DOI: [10.1103/PhysRevD.88.033003](https://doi.org/10.1103/PhysRevD.88.033003)

PACS numbers: 13.40.Em, 13.85.Qk, 14.65.Ha

I. INTRODUCTION

In view of its large mass the top quark is a unique probe of the dynamics that breaks the electroweak gauge symmetry. While the observation of a Higgs boson at the CERN LHC [1] and first measurements of its production and decay channels appear to be consistent with the Standard Model (SM) Higgs mechanism of electroweak symmetry breaking, this mechanism is still far from being validated at high precision. Deviations from the SM are likely to be most pronounced in processes involving top quarks. They may become manifest as deviations of the top quark gauge-boson couplings from the values predicted by the SM (see [2,3] for overviews).

Several studies have established photon radiation in top quark pair production at hadron colliders as a potential probe of anomalous coupling effects [4], which could be improved upon only at a future high-energy electron-positron collider by exploiting final state correlations [5] in top quark pair production. The production of $t\bar{t}\gamma$ final states was first measured at the Tevatron [6], and studies at the LHC are ongoing. While indirect constraints on anomalous electromagnetic couplings from electroweak precision data or flavor physics observables turn out to be very constraining for bottom quarks [7,8], only loose constraints can be obtained in the case of top quarks (see [9,10] for recent studies).

With the hadron collider cross sections for top quark pair production and single-top-quark production being of comparable magnitude, it appears worthwhile to extend the considerations made in [4] to photon radiation in single-top-quark production as a probe of anomalous electromagnetic couplings of the top quark. It is the aim of the present paper to investigate the sensitivity of photon radiation in single-top-quark production events on anomalous electromagnetic couplings of the top quark. In Sec. II, we recall the most general parametrization of the photonic vertex function of the top quark, and its effective field theory expansion defining the top quark electric and magnetic dipole moments, and discuss the parton-level phenomenology of these new operators. Section III

contains numerical results for signal and background processes contributing to single-top-plus-photon production in view of a determination of anomalous couplings in this process. These results are used in Sec. IV to quantify the sensitivity of future LHC data on these couplings. We conclude with Sec. V.

II. ANOMALOUS TOP QUARK COUPLINGS

A. General $t\bar{t}\gamma$ coupling

The most general Lorentz-invariant vertex function describing the interaction of two on-shell top quark and a photon can be written in the form

$$\Gamma_\mu(q^2) = -ie \left\{ \gamma_\mu [F_{1V}(q^2) + F_{1A}(q^2)\gamma_5] + \frac{\sigma_{\mu\nu}}{2m_t} q^\nu [iF_{2V}(q^2) + F_{2A}(q^2)\gamma_5] \right\}, \quad (1)$$

where e is the proton charge, m_t the top mass, $\sigma_{\mu\nu} = i/2[\gamma_\mu, \gamma_\nu]$, and q is the four-momentum of the off-shell photon. The functions $F_i(q^2)$ are called the form factors and in the limit $q^2 \rightarrow 0$ they are physical and related to the static quantities

$$F_{1V}(0) = Q_t, \quad F_{2V}(0) = a_t Q_t, \quad F_{2A}(0) = d_t \frac{2m_t}{e}, \quad (2)$$

where $Q_t = 2/3$ is the top electric charge, a_t and d_t are, respectively, the anomalous magnetic moment and the electric dipole moment of the top. The electric dipole contribution $F_{2A}(q^2)$ violates CP invariance and vanishes in any CP -conserving theory. The form factors in (1) can be computed order by order in perturbation theory; they are known to one loop in the electroweak theory [11] and to two loops in QCD [12]. Standard model values for the static dipole moments can be derived from these form factor results [13]; the standard model prediction for the anomalous magnetic moment of the top quark amounts to $Q_t \cdot a_t \approx 0.02$, while the electric dipole moment is vanishingly small: $d_t < 10^{-30} e \text{ cm}$ [14]. These dipole moments are potentially sensitive to new physics effects in the

top quark sector, which could yield potentially large contributions [2–4,15].

The kinematical situation (all particles on shell) relevant to the static dipole moments (2) cannot be realized for top quarks at a collider experiment. To study the signature of the dipole couplings and to compute sensitivity bounds one adopts an effective Lagrangian approach, where the dipole couplings in Eq. (1) are introduced at tree level via two dimension-5 effective operators of the form

$$\mathcal{L}_{\text{eff}} = -a_t \frac{Q_t e}{4m_t} \bar{t} \sigma_{\mu\nu} t F^{\mu\nu} + i \frac{d_t}{2} \bar{t} \sigma_{\mu\nu} \gamma_5 t F^{\mu\nu}. \quad (3)$$

In this effective field theory framework, Feynman rules for the anomalous coupling of top quarks to photons can be derived. The best constraints on these anomalous couplings can at present be obtained from a combination of the direct production process $p\bar{p} \rightarrow t\bar{t}\gamma$ [6] and flavor observables. They read [10]

$$\begin{aligned} -3.0 < a_t < 0.45, \\ -0.29 \times 10^{-16} e \text{ cm} < d_t < 0.86 \times 10^{-16} e \text{ cm}. \end{aligned} \quad (4)$$

To understand the dependence of production cross sections on the dipole moments, it is illustrative to combine the two real dipole moments a_t and d_t into a single complex dipole moment [16]:

$$c = a_t \frac{Q_t e}{2m_t} - i d_t. \quad (5)$$

With this, the interaction Lagrangian in Eq. (3) can be recast as

$$\mathcal{L}_{\text{eff}} = -\frac{1}{2} [c \bar{t}_L \sigma_{\mu\nu} t_R + c^* \bar{t}_R \sigma_{\mu\nu} t_L] F^{\mu\nu}, \quad (6)$$

where t_R and t_L are, respectively, the right- and left-handed chiral spinor projections. Direct production processes at hadron colliders are not suited to disentangle the contributions from the CP -conserving magnetic dipole moment a_t and the CP -violating electric dipole moment d_t . As a matter of fact, production amplitudes will usually probe the modulus of the complex dipole moment, i.e., the combination

$$|c| = \sqrt{\left(a_t \frac{Q_t e}{2m_t}\right)^2 + d_t^2}, \quad (7)$$

whereas they are almost insensitive to the phase

$$\tan(\varphi_c) = \frac{d_t}{a_t} \frac{2m_t}{Q_t e} \quad (8)$$

that can be regarded also as a measure of CP violation.

B. Top quark dipole moment in single-top-plus-photon production

The measurement of a_t and d_t is extremely challenging because of the very short mean life of the quark that makes

it impossible to measure the two parameters by the interaction with an external electromagnetic field. Bounds on the anomalous couplings of the top can be inferred from the cross section for $t\bar{t}$ pair production and single-top production at the LHC. Their extraction in top quark pair production from $t\bar{t}\gamma$ and $t\bar{t}Z$ final states was investigated in detail in [4]. These measurements can be complemented by single-top-quark production processes, which we study here.

Single-top-quark production at LHC is largely dominated by the t -channel process: $pp \rightarrow t + j$ with a light quark jet in the final state [17,18]. A potential probe of anomalous couplings in the top quark sector thus proceeds through the reaction

$$pp \rightarrow tj\gamma. \quad (9)$$

To quantify the potential effect of an anomalous magnetic moment of the top quark on this process, we first consider the parton-level reaction

$$ub \rightarrow td\gamma \quad (10)$$

at fixed center-of-mass energy, and in the rest frame of the incoming partons.

Cross sections are obtained with a Fortran code generated by FeynArts and FormCalc [19]. The new operators appearing in Eq. (3) are implemented in FeynArts with the Mathematica package FeynRules [20]. Following the above reasoning, we focus our discussion on the CP -conserving coupling $a_t \neq 0$ and set $d_t = 0$. The total cross section σ for the reaction in Eq. (10) can be split in three contributions,

$$\sigma = \sigma_{\text{SM}} + a_t \sigma_a + a_t^2 \sigma_{aa}, \quad (11)$$

where σ_{SM} is the leading-order Standard Model prediction, the term σ_a linear in a_t arises from the interference between the Standard Model and the anomalous amplitudes, whereas the quadratic term σ_{aa} is the self-interference of the anomalous amplitudes.

We observe in Fig. 1 (left) that a contribution from the g -2 coupling gives a photon energy spectrum harder than the SM one because of the growth with \sqrt{s} associated with the dimension-5 operators in Eq. (3). The relative importance of the linear and quadratic terms σ_a and σ_{aa} is illustrated in Fig. 1 (right). It can be seen that for large $|a_t| > 0.1$, the quadratic term σ_{aa} clearly dominates over the interference contribution σ_a . This feature can be understood from the helicity structure of the amplitudes for the Standard Model process and for the anomalous contribution. As a consequence, we expect a bound on a_t to be almost insensitive on the sign and limited by quadratic dependence of the cross section on the anomalous coupling.

As already anticipated in the previous section, analogous results are obtained for a nonzero electric dipole moment

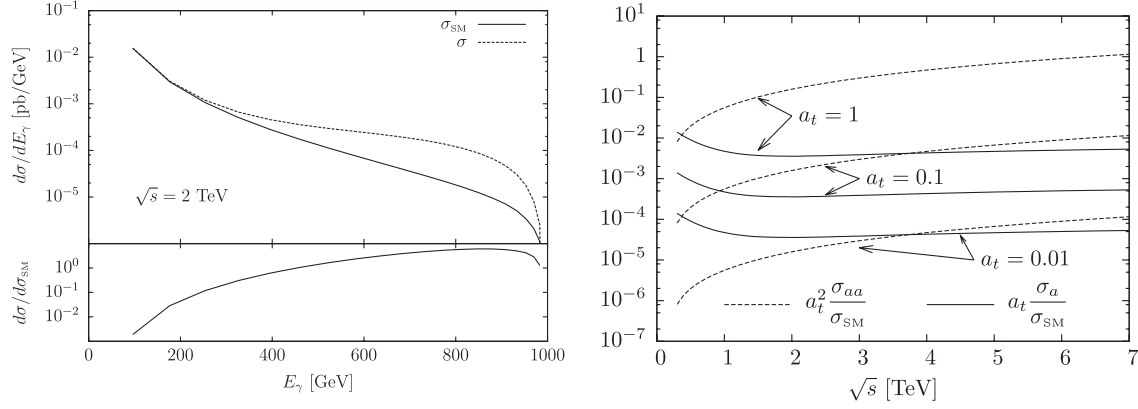


FIG. 1. The parton-level cross section for $ub \rightarrow td\gamma$. Left: photon energy distribution at $\sqrt{s} = 2$ TeV. Standard Model process and anomalous contribution for $a_t = 1$, $d_t = 0$. Right: parton-level cross section as function of the parton-parton center-of-mass energy \sqrt{s} . Ratio of the anomalous terms σ_a and σ_{aa} to the Standard Model process for different values of a_t .

case when the role of the dimensionless parameter a_t is played by $d_t(2m_t/Q_t e)$.

III. NUMERICAL RESULTS FOR SIGNAL AND BACKGROUND PROCESSES

To assess the potential of single-top-plus-photon production at the LHC (with center-of-mass energy of 14 TeV), we concentrate on photon radiation in the t -channel single-top production process, $pp \rightarrow tj\gamma$, followed by $t \rightarrow bW^+$, where the W boson decays into an electron or a muon (τ leptons are ignored). We take into account also t -channel single-top production followed by top radiative decay ($t \rightarrow bl\nu_l\gamma$). The process is combined with its charge conjugate $pp \rightarrow \bar{t}j\gamma$, followed by $\bar{t} \rightarrow \bar{b}W^-$. From now on we will refer to these processes simply as “single-top + γ .” In the final state of the processes

$$pp \rightarrow \gamma l^+ \nu_l b j, \quad pp \rightarrow \gamma l^- \bar{\nu}_l \bar{b} j \quad \text{with } l = e, \mu, \quad (12)$$

we require two jets, one of them tagged as a b -jet, a hard isolated photon, an isolated lepton, and missing energy from the undetected neutrino.

We generate at leading-order parton-level event samples with MadGraph5 [21]. Besides its Standard Model electromagnetic interaction, the top quark couples with the photon also via the effective operators introduced in Eq. (3), by means of a new Madgraph model generated with FeynRules [20]. We assume in general contributions from both the anomalous electric and magnetic dipole moments. In the simulation the top quark mass is $m_t = 173.5$ GeV and all other quarks and leptons masses are set to zero. The single-top cross section is computed in the five-flavor scheme and includes top quark and W decay width effects and full spin correlations. All cross sections for signal and background are computed using CTEQ6L1 parton distribution [22]. The renormalization and factorization scales are chosen event by event to be

$$\mu_F^2 = \mu_R^2 = m_t^2 + \sum_i p_T^2(i), \quad (13)$$

where m_t is the top mass and the index i runs over the visible particles in the final state.

The acceptance cuts for signal and background events are

$$\begin{aligned} p_T(\gamma) &> 100 \text{ GeV}, & p_T(j) &> 20 \text{ GeV}, \\ p_T(b) &> 20 \text{ GeV}, & \cancel{p}_T &> 20 \text{ GeV}, \\ |\eta(\gamma)| &< 2.5, & |\eta(b)| &< 2.5, \\ |\eta(j)| &< 5, & |\eta(l)| &< 2.5, \\ \Delta R(j, b) &> 0.4, & \Delta R(j, l) &> 0.4, \\ \Delta R(j, \gamma) &> 0.4, & \Delta R(l, \gamma) &> 0.4, \\ \Delta R(l, b) &> 0.4, & \Delta R(b, \gamma) &> 0.4, \end{aligned} \quad (14)$$

where $\Delta R^2 = \Delta\Phi^2 + \Delta\eta^2$ is the separation in the rapidity-azimuth plane and \cancel{p}_T is the missing momentum due to the undetected neutrino.

The large cut on the photon transverse momentum enhances the contribution from the anomalous couplings, which grows with the photon energy. As a side effect, it also results in a suppression of Standard Model background processes yielding the same final state signature.

In addition to the cuts listed above, we also require the final state to be consistent with the single-top + γ production. In particular to reduce the background, the invariant mass $m(lb\nu)$ of the b -jet, the charged lepton, and the neutrino should be close to the top mass. We choose to apply the technique in Ref. [23] for the reconstruction of the unmeasured z component of the neutrino momentum $p_z(\nu)$. The transverse momentum of the neutrino is given by the x and y components of the \cancel{E}_T vector, while the z component $p_z(\nu)$ is inferred by imposing a W -boson mass constraint on the lepton-neutrino system.

Since the constraint leads to a quadratic equation for $p_z(\nu)$, in case of two real solutions the smaller one $|p_z|$ is chosen. If the solutions are complex, the neutrino p_x and p_y are rescaled such that the imaginary radical vanishes but keeps the transverse component of the neutrino as close as possible to \cancel{E}_T . In the end we select events with

$$150 \text{ GeV} < m(lb\nu) < 200 \text{ GeV}. \quad (15)$$

The assumption $m(lb\nu) \sim m_t$ does not take into account the possibility of the radiative top decay where $m_t \sim m(lb\nu\gamma)$. However we checked that the contribution to the total cross section arising from radiative top decay is suppressed by the cut on the photon transverse momentum.

A. Signal cross section

Imposing the cuts listed in Eqs. (14) and (15) we obtain cross sections for single-top-plus-photon production at the $\sqrt{s} = 14$ TeV LHC of 9.0 fb for final states involving a t quark and 5.6 fb for final states involving a \bar{t} quark. In the following, we will always add both these

contributions to obtain the single-top-plus-photon production rates.

In Fig. 2 we show various distributions for single-top + γ production at the LHC. To illustrate the magnitude of potential effects, we compare the Standard Model prediction with a prediction including a nonstandard $tt\gamma$ coupling with $a_t = 1.0$, $d_t = 0$. It can be seen that the photon spectrum is considerably harder in the high- p_T region when $a_t \neq 0$. Consequently, $g-2$ effects are enhanced in the configuration where the top quark (or its decay products b and l) are back to back to the photon, as shown in the ΔR distributions.

B. Backgrounds

We distinguish two types of backgrounds: the irreducible background from the Standard Model process $pp \rightarrow (W \rightarrow l\nu_l)bj\gamma$, which yields the identical final state, and potentially reducible backgrounds from various other Standard Model processes that yield different final states that are attributed to the single-top-plus-photon signature due to a misidentification of one or more of the final state objects.

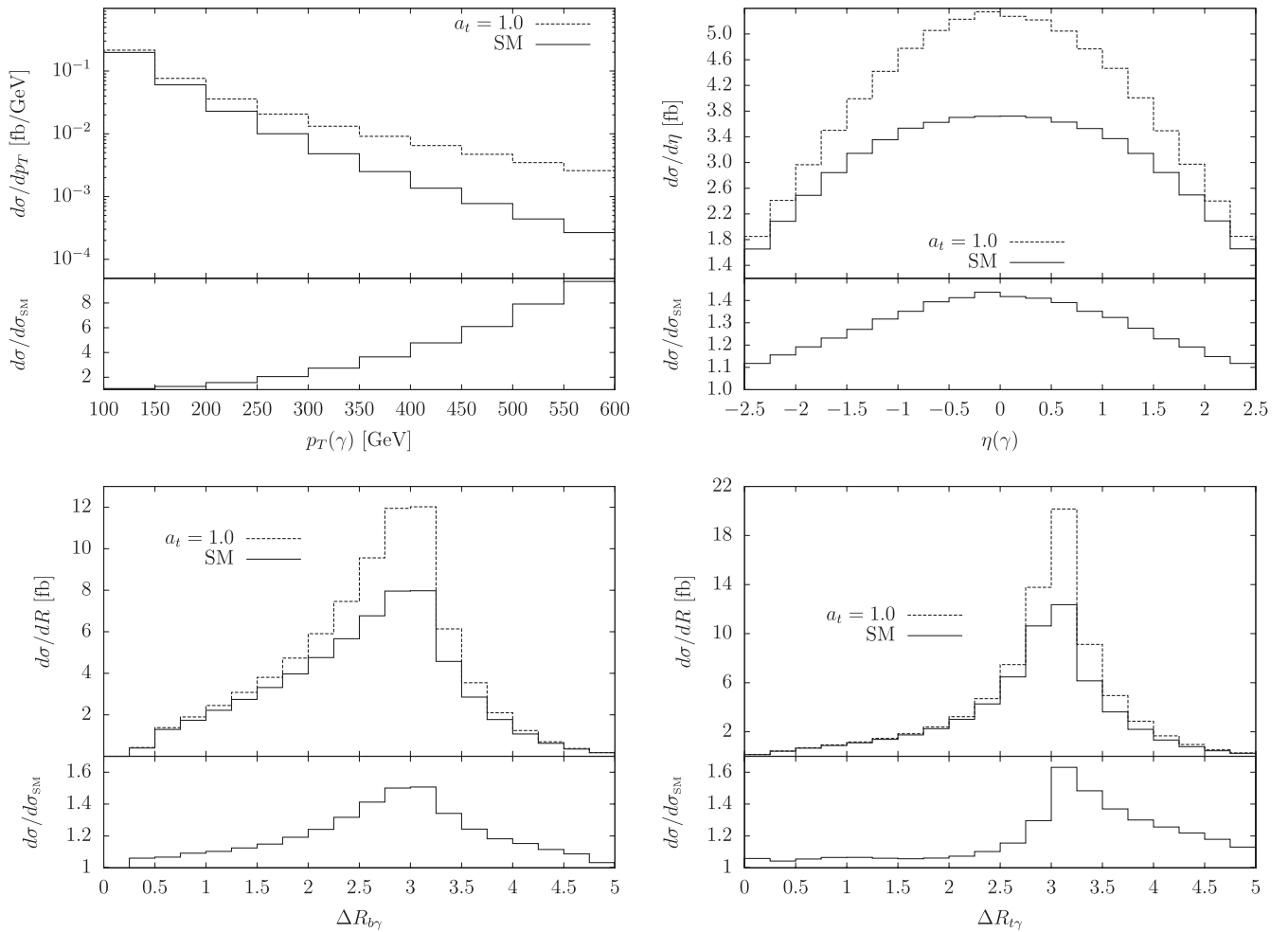


FIG. 2. Kinematical distributions in single-top + γ production at the LHC with $\sqrt{s} = 14$ TeV.

TABLE I. Expected cross section for single-top + γ signal and the most important background processes at the LHC. Photon misidentification probabilities and b -jet mistag rates and efficiencies are included.

| Process | Measurable cross section [fb] |
|-----------------------|-------------------------------|
| single-top + γ | 8.0 |
| $Wbj\gamma$ | $\mathcal{O}(10^{-2})$ |
| $t\bar{t}$ full lep. | 15.0 |
| $W\gamma$ + jets | 1.5 |
| W + jets | 0.4 |
| $t\bar{t}\gamma$ | 0.2 |
| $Z\gamma$ + jets | $\mathcal{O}(10^{-2})$ |
| Z + jets | $\mathcal{O}(10^{-2})$ |

The most important reducible background processes come from light jets faking either a b -jet or photon, or from electrons misidentified as photons. In the analysis we assume a b -jet tagging efficiency of $\varepsilon_b = 60\%$ and a corresponding mistag rate of $\varepsilon_{\text{light}} = 0.1\%$ for a light jet (u, d, s quark or gluon) and $\varepsilon_c = 1\%$ for a c -jet, consistent with typical values assumed by the LHC experiments; see e.g., [24]. We apply the cuts in Eq. (14) where the (mistag) b -jet is chosen randomly.

A potentially dangerous background arises from jets misidentified as photons. To estimate the size of these processes we define a jet fake rate $f_{j\rightarrow\gamma}$ as the probability for a light jet to be misidentified as a photon. The rate $f_{j\rightarrow\gamma}$ is the one used in the experimental measurement of the $W\gamma$ and $Z\gamma$ cross section and the W + jet cross section at ATLAS [25], which estimated it to be $f_{j\rightarrow\gamma} \sim 1/2500$. Similar misidentification rates were reported in the expected performance for the ATLAS detector [26]. Background processes considered are $Wjjj$, $Wbjj$, and $Wbbj$ where a jet with at least $p_T > 100$ GeV fakes a photon (the $Wjjj$ process contributes only if it also yields a mistagged b -jet).

Electrons from W and Z boson decays can be misidentified as photons since the two particles generate similar

electromagnetic signatures. The fake rate $f_{e\rightarrow\gamma}$, defined as the probability for a true electron to be identified as a converted photon, is estimated thorough the Z boson decay $Z \rightarrow ee$ as reported in the measurement of $W\gamma$, $Z\gamma$, $\gamma\gamma$ cross sections [25,27]. The measured rate varies between 2% and 6% and in our case we conservatively assume $f_{e\rightarrow\gamma} \sim 6\%$. Since we require events with a certain amount of missing energy, the background taken into account here is the full leptonic $t\bar{t}$ production, where the two tops decay $t \rightarrow bl^+\nu_l$ and $\bar{t} \rightarrow b\bar{l}^-\bar{\nu}_l$. Processes involving a pair of vector bosons, such as $WWjj$ or $WZjj$, turn out to be irrelevant.

Other kinds of backgrounds result from Z -boson decays to leptons, where one lepton is outside the detector coverage ($|\eta_l| > 2.5$) and fakes missing energy. Here we consider $Zbb\gamma$, $Zbj\gamma$, $Zjj\gamma$, and $t\bar{t}\gamma$. All these kinds of processes are negligible in our case.

Table I summarizes the (Standard Model, without anomalous couplings) signal and background cross sections after the application of the cuts in Eqs. (14) and (15). For the single-top + γ cross section the b -tagging efficiency is included, thereby lowering the total cross section from the parton-level value stated above.

We observe that the signal process is 2 orders of magnitude larger than the irreducible background, and half the sum of all reducible background processes. It is clear that it will be possible to establish the Standard Model single-top-plus-photon process in the region of high photon p_T already with moderate luminosity. However, a detection of anomalous couplings in this process requires a precision measurement of the cross section and of differential distributions. In the following, we use our simulation to determine the sensitivity of future LHC measurements of single-top-plus-photon process on a potential anomalous magnetic moment of the top quark.

IV. BOUNDS FROM FUTURE LHC DATA

We use the shape of the photon transverse momentum distribution to derive quantitative sensitivity bounds that

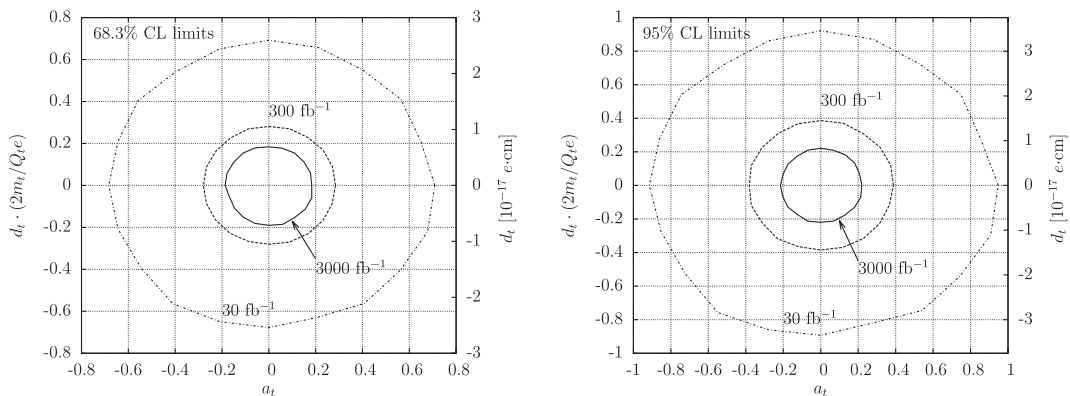


FIG. 3. Bounds on the anomalous dipole moments of the top quark at 68% (left) and 95% (right) confidence level, for LHC operation at $\sqrt{s} = 14$ TeV.

TABLE II. Sensitivity achievable at 95% C.L. in single-top + γ at the LHC ($\sqrt{s} = 14$ TeV) for integrated luminosities of 30 fb^{-1} , 300 fb^{-1} , and 3000 fb^{-1} .

| Coupling | 30 fb^{-1} | 300 fb^{-1} | 3000 fb^{-1} |
|-----------------------------------|----------------------|-----------------------|------------------------|
| a_t | +0.94 -0.92 | +0.39 -0.38 | +0.22 -0.21 |
| $d_t[10^{-17} e \cdot \text{cm}]$ | +3.5 -3.4 | +1.5 -1.5 | +0.83 -0.82 |

can be obtained on the anomalous dipole moments of the top quark. After imposing the cuts in Eqs. (14) and (15), we combine channels with electrons and muons in the final state. We perform a χ^2 test on the distributions and calculate 68.3% and 95% confidence level limits. The dominant backgrounds consist of $t\bar{t}$, $W\gamma$ + jets, and W + jets. Other sources of background are neglected. Limits at the LHC with $\sqrt{s} = 14$ TeV are computed for an integrated luminosity of 30 fb^{-1} (one year of operation), 300 fb^{-1} (integrated luminosity expected from the upcoming run period), and 3000 fb^{-1} (high-luminosity upgrade option). The sensitivity bounds are shown in Fig. 3 and Table II. As already discussed in Sec. II B above, the measurement is insensitive on the sign of the anomalous dipole moments and on the interplay of a_t and d_t due to the dominance of the self-interference term.

Concentrating on the limits at 95% confidence level, we observe that with 30 fb^{-1} only contributions to the dipole moments at order unity could be detected. With higher luminosity, these limits improve towards 0.4 (at 300 fb^{-1}) and 0.2 (at 3000 fb^{-1}). Compared with the current bounds (4), which arise essentially from flavor physics observables and are thus of indirect nature, a significant improvement can be obtained. Depending on the sign of a_t or d_t , the improved constraints with a luminosity of 3000 fb^{-1} can be up to a factor 10 more restrictive than current bounds.

In [4], anticipated limits (for the same luminosity scenarios) from $t\bar{t}\gamma$ final states on the anomalous interactions of the top quarks were expressed in terms of the form

factors $F_{2V}(0)$ and $F_{2A}(0)$ defined in Eq. (2). These limits can be converted in a straightforward manner into limits on the anomalous dipole moments considered here. The limits at 95% confidence level that are obtained by $t\bar{t}\gamma$ production are very similar to those obtained here from single-top-plus-photon production. Both channels are completely independent from each other, and a combination of them could thus further improve the sensitivity.

V. CONCLUSIONS

In this paper, we have demonstrated the sensitivity of single-top-plus-photon production at the LHC on the anomalous dipole moments of the top quark. Contributions from the corresponding effective operators yield a photon transverse momentum spectrum that is harder than what is expected in the Standard Model. By simulating the signal process and all potentially relevant irreducible and reducible backgrounds to it, we have quantified the numerical magnitude of anomalous top quark dipole moments that could be detected in the 14 TeV runs at the LHC with different luminosity scenarios. Our results are summarized in Fig. 3; they demonstrate that the bounds that can be obtained from single-top-plus-photon production are very much comparable in magnitude to those that can be obtained from $t\bar{t}\gamma$ final states [4] and can potentially improve upon existing bounds [9,10] by up to an order of magnitude.

ACKNOWLEDGMENTS

We are very grateful to Rikkert Frederix and Stefano Pozzorini for numerous discussions throughout this project, and to Olivier Mattelaer for help with the MadGraph5 code. This research was supported by the European Commission through the ‘‘LHCPhenoNet’’ Initial Training Network PITN-GA-2010-264564 and by the Swiss National Science Foundation (SNF) under Contract No. 200020-138206.

-
- [1] G. Aad *et al.* (ATLAS Collaboration), *Phys. Lett. B* **716**, 1 (2012); S. Chatrchyan *et al.* (CMS Collaboration), *Phys. Lett. B* **716**, 30 (2012).
 - [2] H. Murayama and M. E. Peskin, *Annu. Rev. Nucl. Part. Sci.* **46**, 533 (1996).
 - [3] C. T. Hill and E. H. Simmons, *Phys. Rep.* **381**, 235 (2003); **390**, 553(E) (2004).
 - [4] U. Baur, A. Juste, L. H. Orr, and D. Rainwater, *Phys. Rev. D* **71**, 054013 (2005).
 - [5] G. A. Ladinsky and C. P. Yuan, *Phys. Rev. D* **49**, 4415 (1994); B. Grzadkowski and Z. Hioki, *Nucl. Phys.* **B585**, 3 (2000); Z. H. Lin, T. Han, T. Huang, J. X. Wang, and X. Zhang, *Phys. Rev. D* **65**, 014008 (2001).
 - [6] T. Aaltonen *et al.* (CDF Collaboration), *Phys. Rev. D* **84**, 031104 (2011).
 - [7] G. Altarelli, R. Barbieri, and S. Jadach, *Nucl. Phys.* **B369**, 3 (1992); **B376**, 444(E) (1992); G. Altarelli, R. Barbieri, and F. Caravaglios, *Nucl. Phys.* **B405**, 3 (1993).
 - [8] O. J. P. Eboli, M. C. Gonzalez-Garcia, and S. F. Novaes, *Phys. Lett. B* **415**, 75 (1997).
 - [9] J. F. Kamenik, M. Papucci, and A. Weiler, *Phys. Rev. D* **85**, 071501 (2012).
 - [10] A. O. Bouzas and F. Larios, *Phys. Rev. D* **87**, 074015 (2013).
 - [11] W. Hollik, *Fortschr. Phys.* **38**, 165 (1990); A. Czarnecki, B. Krause, and W. J. Marciano, *Phys. Rev. Lett.* **76**, 3267

- (1996); J. Bernabeu, J. Vidal, and G.A. Gonzalez-Sprinberg, *Phys. Lett. B* **397**, 255 (1997).
- [12] W. Bernreuther, R. Bonciani, T. Gehrmann, R. Heinesch, T. Leineweber, P. Mastrolia, and E. Remiddi, *Nucl. Phys. B* **706**, 245 (2005); **712**, 229 (2005); W. Bernreuther, R. Bonciani, T. Gehrmann, R. Heinesch, T. Leineweber, and E. Remiddi, *ibid.* **723**, 91 (2005).
- [13] W. Bernreuther, R. Bonciani, T. Gehrmann, R. Heinesch, T. Leineweber, P. Mastrolia, and E. Remiddi, *Phys. Rev. Lett.* **95**, 261802 (2005).
- [14] A. Soni and R.M. Xu, *Phys. Rev. Lett.* **69**, 33 (1992).
- [15] T. Ibrahim and P. Nath, *Phys. Rev. D* **82**, 055001 (2010); **84**, 015003 (2011).
- [16] A. Czarnecki and W.J. Marciano, in *Lepton Dipole Moments* (World Scientific, Singapore, 2010), p. 11.
- [17] S. Chatrchyan *et al.* (CMS Collaboration), *J. High Energy Phys.* **12** (2012) 035.
- [18] G. Aad *et al.* (ATLAS Collaboration), *Phys. Lett. B* **717**, 330 (2012).
- [19] T. Hahn, *Comput. Phys. Commun.* **140**, 418 (2001); T. Hahn and M. Perez-Victoria, *Comput. Phys. Commun.* **118**, 153 (1999).
- [20] N.D. Christensen and C. Duhr, *Comput. Phys. Commun.* **180**, 1614 (2009).
- [21] J. Alwall, M. Herquet, F. Maltoni, O. Mattelaer, and T. Stelzer, *J. High Energy Phys.* **06** (2011) 128.
- [22] J. Pumplin, D.R. Stump, J. Huston, H.L. Lai, P.M. Nadolsky, and W.K. Tung, *J. High Energy Phys.* **07** (2002) 012.
- [23] J. Bauer, Report No. CERN-THESIS-2010-146.
- [24] S. Chatrchyan *et al.* (CMS Collaboration), *JINST* **8**, P04013 (2013).
- [25] G. Aad *et al.* (ATLAS Collaboration), *Phys. Rev. D* **87**, 112003 (2013).
- [26] G. Aad *et al.* (ATLAS Collaboration), *arXiv:0901.0512*.
- [27] G. Aad *et al.* (ATLAS Collaboration), *J. High Energy Phys.* **01** (2013) 086.